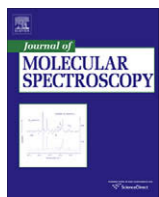




Contents lists available at ScienceDirect

Journal of Molecular Spectroscopy

journal homepage: www.elsevier.com/locate/jms



Feature Article

High-resolution infrared spectroscopy of $^{15}\text{N}_2^{16}\text{O}$ in the 3500–9000 cm^{-1} region

B. Gao, C.-Y. Wang, Y. Lu, A.-W. Liu*, S.-M. Hu

Hefei National Laboratory for Physical Sciences at Microscale, University of Science and Technology of China, Hefei 230026, China

ARTICLE INFO

Article history:

Received 14 October 2009

In revised form 27 October 2009

Available online 1 November 2009

Keywords:

Nitrous oxide

$^{15}\text{N}_2^{16}\text{O}$

Vibration–rotation spectroscopy

Line positions

Spectroscopic parameters

ABSTRACT

The Fourier-transform absorption spectrum of $^{15}\text{N}_2^{16}\text{O}$ -enriched nitrous oxide has been recorded at the Doppler limited resolution in the spectral range 3500–9000 cm^{-1} . 6523 Transitions of $^{15}\text{N}_2^{16}\text{O}$ were observed and assigned based on the global effective Hamiltonian model. The band-by-band analysis led to the determination of the ro-vibrational parameters of a total of 65 bands. Among these bands, 39 are newly observed, and the rotational analysis of 26 others were significantly extended and improved.

© 2009 Elsevier Inc. All rights reserved.

1. Introduction

Nitrous oxide (N_2O) is a minor constituent of the earth atmosphere, but it plays important roles in atmospheric chemistry as a greenhouse gas and in stratospheric ozone depletion. Isotopic measurements of N_2O have provided an invaluable insight into understanding its atmospheric sources and sinks. We have undertaken a systematic study of the absorption spectrum of the main isotopologues of nitrous oxide [1–4] in the middle and near infrared regions. The $^{15}\text{N}_2^{16}\text{O}$ isotopologue has a very small natural abundance (0.0013%), but the line parameters of this isotopologue can be useful for a better atmospheric spectra simulation and also for developing theoretical models describing the isotopic substitution effect on the spectral line parameters.

To our knowledge only two works are available in the literature for the line positions measurements of this isotopic species. Amiot [5] studied the spectrum of the $^{15}\text{N}_2^{16}\text{O}$ isotopologue in the 1750–6000 cm^{-1} region, which resulted in 64 bands and 44 vibrational levels. Nine vibrational levels are included in Toth's work [6]. No line parameters of $^{15}\text{N}_2^{16}\text{O}$ have been presented in HITRAN [7] or GEISA [8] database.

In this work, 6523 lines of 65 bands have been studied between 3500 and 9000 cm^{-1} for the $^{15}\text{N}_2^{16}\text{O}$ isotopologue. The paper is organized as following: in Section 2, we present briefly the experimental conditions employed to measure the spectra. In Section 3,

the vibrational assignments and a band-by-band rotational analysis are presented. The results will be discussed in Section 4.

2. Experimental details

The $^{15}\text{N}_2^{16}\text{O}$ enriched nitrous oxide sample was purchased from Icon Services Inc. The absorption spectrum was recorded by a Bruker IFS 120HR interferometer equipped with a multi-pass gas cell with an adjustable path length. The whole interference chamber was evacuated to less than 0.4 mbar to reduce background absorption and interference from atmospheric gases. Because of the wide spectral range and the large variations in absorption band intensities, different experimental conditions were applied for the measurements, as listed in Table 1. The gas sample pressure was measured using two capacitance manometers (MKS Baratron 627B) with 1 and 20 Torr full-scale ranges and 0.15% accuracy. Different optical filters were applied to improve the signal-to-noise ratio and to allow the high-resolution measurements. The line positions were calibrated using the absorption lines of water and carbon dioxide. Their values were taken from the Hitran2008 database [7]. The accuracy of the unblended and not-very-weak lines is estimated to be better than 0.001 cm^{-1} . Overview spectra of 556 enriched sample in the whole studied region is presented in Fig. 1.

3. Ro-vibrational analysis

3.1. Vibrational assignment

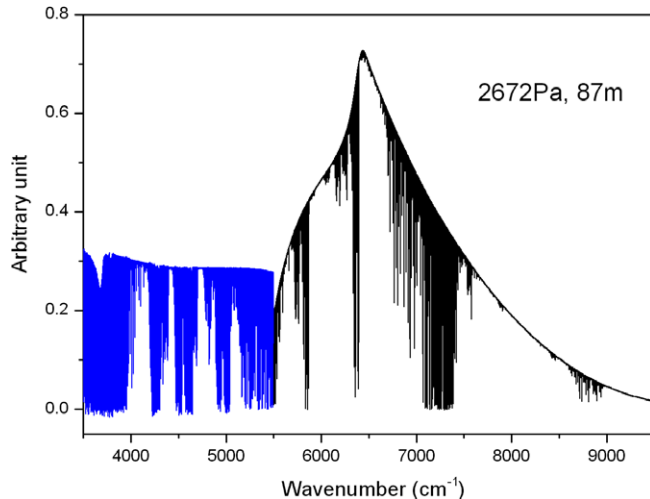
The observed transitions were assigned based on the predictions of the effective ro-vibration Hamiltonian for $^{15}\text{N}_2^{16}\text{O}$ obtained

* Corresponding author. Address: University of Science and Technology of China, Hefei National Laboratory for Physical Sciences at Microscale, JinZhai Road No. 96, 230026 Hefei, China. Fax: +86 551 3602969.

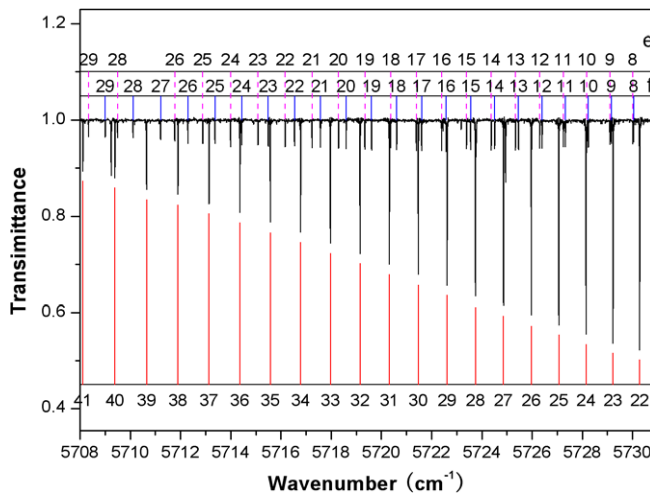
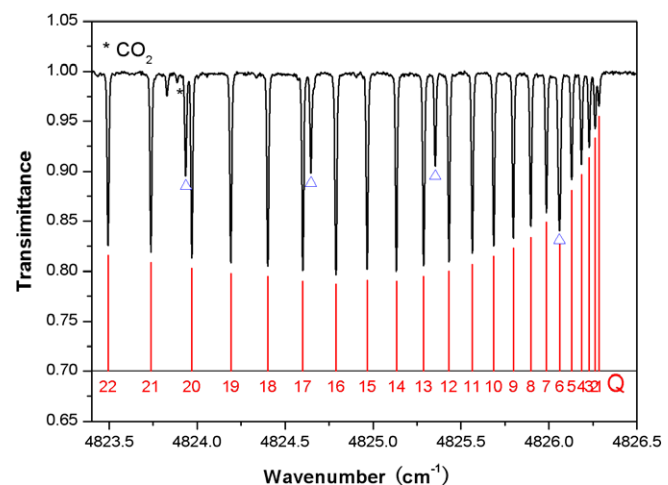
E-mail address: awliu@ustc.edu.cn (A.-W. Liu).

Table 1Experimental conditions of $^{15}\text{N}_2^{16}\text{O}$ enriched nitrous oxide sample.

Range (cm^{-1})	Pressure (Pa)	Detector	Path length (m)	Resolution (cm^{-1})	Temperature (K)
3300–4300	108	InSb	15	0.006	296
3300–4300	534	InSb	15	0.006	291
3300–4300	1332	InSb	15	0.006	293
4100–5000	108	InSb	15	0.008	298
4100–5000	534	InSb	15	0.008	292
4100–5000	1332	InSb	15	0.008	295
5000–6300	534	InSb	15	0.010	292
5000–6300	1332	InSb	15	0.010	294
2100–9000	1336	InSb	87	0.015	292
5500–9050	1336	Ge	87	0.017	296

**Fig. 1.** The Fourier-transform absorption spectrum of $^{15}\text{N}_2^{16}\text{O}$ in the 3500–9000 cm^{-1} region. The spectrum was recorded at a pressure of 1336 Pa and an equivalent absorption path length of 87 m.

in Ref. [10]. The effective Hamiltonian we adopted is based on a polyad structure that results from the approximate relations between the harmonic frequencies $\omega_3 \approx 2\omega_1 \approx 4\omega_2$. Since the mixing between the (V_1, V_2^l, V_3) states may be strong, the vibrational energy levels are labeled using the triplet ($P = 2V_1 + V_2 + 4V_3$, l_2 , i) where the index i increases with energy. In the studied region,

**Fig. 2.** The P -branch of the $22^01e - 00^00e$ $\Sigma-\Sigma$ and the $15^11 - 01^10$ $\Pi-\Pi$ bands of $^{15}\text{N}_2^{16}\text{O}$ isotopologue centered at 5750.7230 cm^{-1} and 5736.8392 cm^{-1} , respectively. And the rotational assignments are presented. The spectrum was recorded at a pressure of 1332 Pa and an equivalent absorption path length of 15 m.**Fig. 3.** The Q -branch of the $0112f - 00^00e$ $\Pi-\Sigma$ cold band centered at 4826.2957 cm^{-1} and the rotational assignments are presented. The spectrum was recorded at a pressure of 1332 Pa and an equivalent absorption path length of 15 m. The lines marked by open triangle correspond to the $32^00e - 00^00e$ band transitions.

the spectrum is mostly dominated by cold bands ($\Delta P \geq 6$) of $^{15}\text{N}_2^{16}\text{O}$ species.

The analyzed bands of $^{15}\text{N}_2^{16}\text{O}$, include 59 parallel ($\Delta l_2 = 0$) bands ($43\Sigma-\Sigma$, $12\Pi-\Pi$, $(4\Delta-\Delta)$, 6 perpendicular ($\Delta l_2 = 1$) bands ($4\Pi-\Sigma$, $2\Sigma-\Pi$). Fig. 2 shows the P -branch of $22^01e - 00^00e$ and $15^11 - 01^10$ bands of $^{15}\text{N}_2^{16}\text{O}$ isotopologue centered at

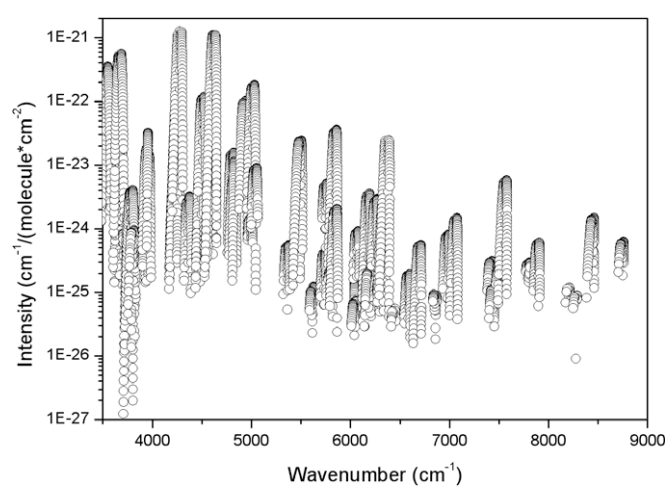
**Fig. 4.** A list of the transitions for $^{15}\text{N}_2^{16}\text{O}$ between 3500 and 9000 cm^{-1} as predicted by the effective Hamiltonian [10]. Note logarithmic scale is used for line intensities.

Table 2

Spectroscopic parameters (in cm^{-1}) of the ro-vibrational bands of $^{15}\text{N}_2^{16}\text{O}$ that were assigned in the FTS spectra between 3500 and 9050 cm^{-1} . The cold and hot bands are listed and ordered according to their ΔG_v values.

$V_1 V_2^l V_3$	G_v	B_v	$D_v \times 10^7$	
<i>Lower state constants</i>				
00 ⁰ 0e	0.0		0.4048602	1.6356
01 ¹ 0e	571.894		0.4050021	1.6560
01 ¹ 0f	571.894		0.4057617	1.6638
02 ⁰ 0e	1136.453		0.405741	2.294
02 ² 0e	1143.961		0.405913	1.112
10 ⁰ 0e	1265.33383		0.403153720	1.627990
11 ¹ 0e	1842.40670		0.403318600	1.637500
11 ¹ 0f	1842.40670		0.404167000	1.620000
ΔG_v^a	Type	Bands ^b	G_v	B_v
3528.751296(84)	$\Pi-\Pi$	23 ¹ 0f – 01 ¹ 0f	4100.645296(84)	0.40620275(39)
3528.751696(84)		23 ¹ 0e – 01 ¹ 0e	4100.645696(84)	0.40392985(34)
3538.480799(68)	$\Sigma-\Sigma$	22 ⁰ 0e – 0000e	3538.480799(68)	0.40475049(25)
3538.4830(1)		14 ⁰ 0e – 00 ⁰ 0e ^A		0.4047477(7)
3666.665449(70)	$\Sigma-\Sigma$	40 ⁰ 0e – 10 ⁰ 0e	4931.999279(70)	0.40063350(33)
3673.27453(14)	$\Delta-\Delta$	32 ² 0e – 02 ² 0e	4817.23553(14)	0.40325546(64)
3673.722695(52)	$\Pi-\Pi$	31 ¹ 0f – 01 ¹ 0f	4245.616695(52)	0.40363262(17)
3673.7249(1)		23 ¹ 0f – 01 ¹ 0f ^A		0.4036327(2)
3673.722857(77)		31 ¹ 0e – 01 ¹ 0e	4245.616857(77)	0.40193568(25)
3673.7249(1)		23 ¹ 0e – 01 ¹ 0e ^A		0.4019357(7)
3673.7229(29)		31 ¹ 0f – 01 ¹ 0e	4245.6169(29)	0.403637(30)
3674.712243(36)	$\Sigma-\Sigma$	14 ⁰ 0e – 00 ⁰ 0e	3674.712243(36)	0.402375262(91)
3674.7146(1)		22 ⁰ 0e – 00 ⁰ 0e ^A		0.4023755(1)
3709.4469(11)	$\Sigma-\Pi$	00 ⁰ 2e – 01 ¹ 0f	4281.3409(11)	0.3983672(93)
3774.236658(93)	$\Sigma-\Sigma$	30 ⁰ 0e – 00 ⁰ 0e	3774.236658(93)	0.39990956(17)
3774.2399(1)		30 ⁰ 0e – 00 ⁰ 0e ^A		0.3999102(3)
3791.068648(88)	$\Pi-\Pi$	31 ¹ 0f – 01 ¹ 0f	4362.962648(88)	0.40124128(27)
3791.0712(1)		31 ¹ 0f – 01 ¹ 0f ^A		0.4012398(2)
3791.068675(76)		31 ¹ 0e – 01 ¹ 0e	4362.962675(76)	0.40011017(21)
3791.0712(1)		31 ¹ 0e – 01 ¹ 0e ^A		0.4001099(1)
3791.06913(50)		31 ¹ 0f – 01 ¹ 0e	4362.96313(50)	0.4012327(63)
3804.82425(17)	$\Delta-\Delta$	32 ² 0e – 0220e	4948.78525(17)	0.4013312(45)
3939.98637(32)	$\Sigma-\Pi$	12 ⁰ 1e – 01 ¹ 0f	4511.88037(32)	0.4008972(11)
3939.98640(14)		12 ⁰ 1e – 01 ¹ 0e	4511.88040(14)	0.40089945(56)
3957.741894(71)	$\Pi-\Sigma$	11 ¹ 1e – 00 ⁰ 0e	3957.741894(71)	0.40011527(28)
3957.7443(1)		11 ¹ 1e – 00 ⁰ 0e ^A		0.400115(3)
3957.74196(17)		11 ¹ 1f – 00 ⁰ 0e	3957.74196(17)	0.40093964(35)
3957.7443(1)		11 ¹ 1f – 00 ⁰ 0e ^A		0.400940 (2)
4227.65505(35)	$\Delta-\Delta$	02 ² 1e – 02 ² 0e	5371.61605(35)	0.3995610(17)
4228.419412(99)	$\Sigma-\Sigma$	02 ⁰ 2e – 02 ⁰ 0e	5364.872412(99)	0.39939121(26)
4229.789828(73)	$\Sigma-\Sigma$	10 ⁰ 2e – 10 ⁰ 0e	5495.123658(73)	0.39664226(19)
4254.4017(10)	$\Pi-\Pi$	01 ¹ 2e – 01 ¹ 0f	4826.2957(10)	0.3986013(86)
4254.402128(60)		01 ¹ 2f – 01 ¹ 0f	4826.296128(60)	0.399322875(88)
4254.4037(1)		01 ¹ 2f – 01 ¹ 0f ^A		0.3993226(4)
4254.402140(71)		01 ¹ 2e – 01 ¹ 0e	4826.296140(71)	0.39859247(11)
4254.4037(1)		01 ¹ 2e – 01 ¹ 0e ^A		0.3985925(5)
4254.40269(63)		01 ¹ 2f – 01 ¹ 0e	4826.29669(63)	0.3993191(57)
4281.340720(47)	$\Sigma-\Sigma$	00 ⁰ 2e – 00 ⁰ 0e	4281.340720(47)	0.398367192(60)
4281.3412(2)		00 ⁰ 2e – 00 ⁰ 0e ^A		0.3983675(2)
4362.96186(20)	$\Pi-\Sigma$	31 ¹ 0e – 00 ⁰ 0e	4362.96186(20)	0.40010976(57)
4362.96248(59)		31 ¹ 0f – 00 ⁰ 0e	4362.96248(59)	0.4012405(24)
4364.18901(12)	$\Sigma-\Sigma$	04 ⁰ 1e – 00 ⁰ 0e	4364.18901(12)	0.40339445(61)
4479.40895(27)	$\Delta-\Delta$	14 ² 1e – 02 ² 0e	5623.16995(27)	0.4018475(12)
4495.352552(52)	$\Pi-\Pi$	13 ¹ 1f – 01 ¹ 0f	5067.246552(52)	0.40211047(13)
4495.3535(3)		13 ¹ 1f – 01 ¹ 0f ^A		0.4021129 (14)
4495.35330(14)		13 ¹ 1e – 01 ¹ 0e	5067.24730(14)	0.40058138(31)
4495.3535(3)		13 ¹ 1e – 01 ¹ 0e ^A		0.400583(1)
4511.88041(15)	$\Sigma-\Sigma$	12 ⁰ 1e – 00 ⁰ 0e	4511.88041(15)	0.40089427(42)
4511.8808(1)		12 ⁰ 1e – 00 ⁰ 0e ^A		0.4009027(7)
4584.13246(12)	$\Sigma-\Sigma$	30 ⁰ 1e – 10 ⁰ 0e	5849.46629(12)	0.39663727(71)
4614.269532(80)	$\Sigma-\Sigma$	22 ⁰ 1e – 02 ⁰ 0e	5750.722532(80)	0.39918429(25)
<i>Observed lines</i>				
			n/N^c	RMS $\times 10^3$
			76/86	0.24
			80/90	0.23
			112/116	0.31
			/57	0.18
			74/80	0.27
			37/45	0.49
			93/104	0.19
			/52	0.21
			97/104	0.30
			/53	0.22
			9/14	0.88
			/88	0.1
			8/10	0.64
			86/86	0.29
			/80	0.34
			102/104	0.30
			/46	0.26
			96/110	0.28
			/56	0.09
			50/52	0.56
			/36	0.3
			54/58	1.29
			83/94	0.45
			78/83	0.33
			13/19	0.73
			94/113	0.27
			/57	0.34
			93/117	0.31
			/59	0.4
			13/21	0.58
			95/100	0.21
			/61	0.58
			35/50	0.53
			28/35	0.83
			84/90	0.45
			39/49	0.87
			88/104	0.23
			/48	0.7
			87/98	0.65
			/48	0.7
			92/98	0.73
			/73	0.46
			73/80	0.42
			64/71	0.34

Table 2 (continued)

$V_1 V_2^l V_3$		G_v		B_v		$D_v \times 10^7$		
4622.884571(82)	$\Pi-\Pi$	$21^11e - 01^10e$	5194.778571(82)	0.39847985(24)	1.5968(18)	0.349(36)	R57/P59	75/92 0.21
4622.8860(1)		$21^11e - 01^10e^A$		0.3984794(3)	1.589(2)		R41/P41	/59 0.34
4622.88503(11)		$21^11f - 01^10f$	5194.77903(11)	0.39940993(20)	1.52005(74)		R56/P58	74/90 0.37
4622.8860(1)		$21^11f - 01^10f^A$		0.3994112(3)	1.525(2)		R42/P41	/59 0.38
4625.604249(50)	$\Sigma-\Sigma$	$20^01e - 00^00e$	4625.604249(50)	0.39822187(12)	1.57392(67)	0.2784(99)	R63/P72	119/128 0.25
4625.6059(2)		$20^01e - 00^00e^A$		0.3982207(3)	1.562(1)		R57/P51	/61 0.9
4807.132821(68)	$\Sigma-\Sigma$	$32^00e - 00^00e$	4807.132821(68)	0.40298620(33)	3.9167(35)	14.84(10)	R51/P51	90/101 0.30
4826.295651(64)	$\Pi-\Sigma$	$01^12e - 00^00e$	4826.295651(64)	0.39859217(16)	1.64384(78)		R47/P47	89/92 0.29
4826.29570(18)		$01^12f - 00^00e$	4826.29570(18)	0.39932389(37)	1.6565(13)		Q55	51/55 0.57
4826.297(1)		$01^12f - 00^00e^A$		0.399323(8)	1.615(80)		Q28	/20 0.37
4931.999863(71)	$\Sigma-\Sigma$	$40^00e - 00^00e$	4931.999863(71)	0.40063098(24)	2.2991(18)	2.623(37)	R59/P53	107/112 0.34
4932.0014(1)		$32^00e - 00^00e^A$		0.4006308(6)	2.302(10)	3.0(4)	R40/P41	/79 0.36
4993.70283(38)	$\Sigma-\Sigma$	$50^00e - 10^00e$	6259.03666(38)	0.3973419(17)	0.868(15)		R32/P29	38/46 0.73
5019.08262(13)	$\Sigma-\Sigma$	$40^00e - 00^00e$	5019.08262(13)	0.39848770(28)	1.2447(11)		R68/P55	103/120 0.67
5019.0832(1)		$40^00e - 00^00e^A$		0.3984934(6)	1.303(9)	1.5(3)	R42/P45	/77 0.42
5042.193693(82)	$\Pi-\Pi$	$41^10e - 01^10e$	5614.087693(82)	0.39863676(27)	1.4106(16)		R40/P42	59/66 0.29
5042.193920(96)		$41^10f - 01^10f$	5614.087920(96)	0.39999816(30)	1.1867(17)		R42/P44	69/76 0.36
5364.87171(24)	$\Sigma-\Sigma$	$02^02e - 00^00e$	5364.87171(24)	0.39940866(90)	2.3883(63)		R39/P40	69/72 1.0
5473.40506(27)	$\Pi-\Pi$	$11^12e - 01^10e$	6045.29906(27)	0.39690741(93)	1.6200(62)		R43/P45	44/78 0.64
5473.40530(22)		$11^12f - 01^10f$	6045.29930(22)	0.39771080(78)	1.6257(51)		R41/P41	44/78 0.54
5495.124118(97)	$\Sigma-\Sigma$	$10^02e - 00^00e$	5495.124118(97)	0.39664099(19)	1.60762(67)		R53/P58	109/112 0.54
5495.1273(1)		$10^02e - 00^00e^A$		0.3966400 (3)	1.602(2)		R40/P39	/59 0.37
5615.48796(12)	$\Sigma-\Sigma$	$22^01e - 00^00e$	5615.48796(12)	0.40166104(77)	3.8183(92)		R28/P30	53/53 0.39
5736.83903(12)	$\Pi-\Pi$	$15^11f - 01^10f$	6308.73303(12)	0.40048115(42)	2.0001(28)		R39/P39	68/77 0.43
5736.83924(13)		$15^11e - 01^10e$	6308.73324(13)	0.39884384(46)	1.9355(31)		R39/P38	63/73 0.45
5750.72307(17)	$\Sigma-\Sigma$	$22^01e - 00^00e$	5750.72307(17)	0.39919554(43)	2.2280(20)		R55/P57	97/113 0.87
5750.7249(2)		$22^01e - 00^00e^A$		0.3992018(8)	2.276(6)		R36/P31	/51 0.62
5801.18756(27)	$\Sigma-\Sigma$	$40^01e - 10^00e$	7066.52139(27)	0.3952263(11)	1.2188(73)		R39/P24	36/51 0.76
5849.46763(11)	$\Sigma-\Sigma$	$30^01e - 00^00e$	5849.46763(11)	0.39663089(21)	1.44198(72)		R68/P57	111/115 0.63
5849.4703(1)		$30^01e - 00^00e^A$		0.3966336(3)	1.457(1)		R46/P44	/85 0.5
5849.46732(4)		$30^01e - 00^00e^L$		0.3966341(2)	1.463(2)			/43
5852.79489(12)	$\Pi-\Pi$	$31^11e - 01^10e$	6424.68889(12)	0.39692081(23)	1.50633(85)		R57/P50	70/85 0.48
5852.79499(15)		$31^11f - 01^10f$	6424.68899(15)	0.39800680(36)	1.3746(17)		R49/P50	71/93 0.52
6045.29833(61)	$\Pi-\Sigma$	$11^12f - 00^00e$	6045.29833(61)	0.3977134(27)	1.639(21)		Q37	25/33 0.79
6045.29893(38)		$11^12e - 00^00e$	6045.29893(38)	0.3969081(22)	1.643(23)		R24/P32	36/46 0.95
6067.15761(19)	$\Sigma-\Sigma$	$42^00e - 00^00e$	6067.15761(19)	0.40117111(13)	3.688(21)	10.16(90)	R39/P39	61/70 0.54
6180.791268(40)	$\Sigma-\Sigma$	$50^00e - 00^00e$	6180.791268(40)	0.39878994(18)	2.2484(18)	2.866(49)	R50/P52	102/103 0.18
6180.79113(7)		$50^00e - 00^00e^L$		0.3987898(5)	2.241(7)	2.5(3)		/72
6185.46487(22)	$\Pi-\Pi$	$51^10e - 01^10e$	6757.35887(22)	0.39836708(79)	1.8540(53)		R38/P41	45/48 0.71
6185.46460(23)		$51^10f - 01^10f$	6757.35860(23)	0.40037751(97)	1.8670(79)		R39/P41	41/49 0.69
6259.035647(41)	$\Sigma-\Sigma$	$50^00e - 00^00e$	6259.035647(41)	0.39734849(22)	0.9709(26)	3.429(84)	R47/P50	92/98 0.17
6259.03542(7)		$50^00e - 00^00e^L$		0.3973491(5)	0.979(7)	3.9(3)		/66
6300.51055(32)	$\Sigma-\Sigma$	$02^03e - 02^00e$	7436.96355(32)	0.3962111(25)	2.270(35)		R26/P28	34/37 0.88
6339.47749(11)	$\Pi-\Pi$	$01^13f - 01^10f$	6911.37149(11)	0.39609638(27)	1.6494(12)		R47/P50	37/89 0.26
6339.4670(6)		$01^13f - 01^10f^L$		0.39535(2)	1.2(4)			/19
6339.47750(16)		$01^13e - 01^10e$	6911.37150(16)	0.39537803(33)	1.6351(13)		R47/P51	41/92 0.40
6339.4674(5)		$01^13e - 01^10e^L$		0.39607(3)	1.2(5)			/14
6379.858650(85)	$\Sigma-\Sigma$	$00^03e - 00^00e$	6379.858650(85)	0.39511246(11)	1.61983(31)		R66/P63	72/88 0.32
6379.8622(1)		$00^03e - 00^00e^A$		0.3951133(4)	1.626(3)		R35/P40	/67 0.49
6379.858640(9)		$00^03e - 00^00e^L$	0.39511266(7)	1.625(1)	0.18(4)		/70	
6438.85415(49)	$\Sigma-\Sigma$	$04^02e - 00^00e$	6438.85415(49)	0.4002880(29)	4.047(33)		R27/P29	17/18 0.57
6586.58618(12)	$\Sigma-\Sigma$	$12^02e - 00^00e$	6586.58618(12)	0.39772535(74)	2.392(10)	3.22(37)	R43/P39	71/79 0.43
6700.441797(57)	$\Sigma-\Sigma$	$20^02e - 00^00e$	6700.441797(57)	0.39495338(16)	1.55855(86)		R49/P51	85/98 0.28
6700.4416(1)		$20^02e - 00^00e^L$		0.3949532(8)	1.556(9)			/42
6857.76752(35)	$\Sigma-\Sigma$	$32^01e - 00^00e$	6857.76752(35)	0.3999201(29)	4.552(47)		R23/P25	51/51 0.95
6980.939068(82)	$\Sigma-\Sigma$	$40^01e - 00^00e$	6980.939068(82)	0.39745676(56)	2.2586(92)	3.67(40)	R37/P41	74/79 0.28
6980.937(1)		$40^01e - 00^00e^L$		0.397466(6)	2.35(8)			/16
7066.521829(56)	$\Sigma-\Sigma$	$40^01e - 00^00e$	7066.521829(56)	0.39522770(40)	1.2546(64)	1.25(27)	R51/P50	72/101 0.21
7066.5216(1)		$40^01e - 00^00e^L$		0.3952277(7)	1.237(7)			/42
7420.40743(23)	$\Sigma-\Sigma$	$60^00e - 00^00e$	7420.40743(23)	0.3968644(11)	2.0221(97)		R33/P34	48/59 0.72
7436.96288(27)	$\Sigma-\Sigma$	$02^03e - 00^00e$	7436.96288(27)	0.3962323(12)	2.433(10)		R37/P34	46/58 0.82

(continued on next page)

Table 2 (continued)

$V_1 V_2^l V_3$	G_v		B_v		$D_v \times 10^7$			
7495.65242(80)	$\Sigma-\Sigma$	$52^00e - 00^00e$	7495.65242(80)	0.3965581(53)	0.810(73)	R25/P27	29/38	1.4
7568.258981(55)	$\Sigma-\Sigma$	$10^03e - 00^00e$	7568.258981(55)	0.39337857(12)	1.59944(51)	R54/P55	95/108	0.29
7568.25825(7)		$10^03e - 00^00e^l$		0.3933787(3)	1.596(3)		/51	
7799.56128(57)	$\Sigma-\Sigma$	$22^02e - 00^00e$	7799.56128(57)	0.3960200(47)	1.321(75)	R23/P25	34/40	1.1
7897.69897(15)	$\Sigma-\Sigma$	$30^02e - 00^00e$	7897.69897(15)	0.39335804(61)	1.4399(47)	R41/P39	65/79	0.60
8201.81876(66)	$\Sigma-\Sigma$	$50^01e - 00^00e$	8201.81876(66)	0.3956015(33)	2.510(35)	R28/P28	8/16	0.52
8278.0781(11)	$\Sigma-\Sigma$	$50^01e - 00^00e$	8278.0781(11)	0.3942205(69)	1.937(96)	R21/P26	8/18	0.90
8450.30549(14)	$\Sigma-\Sigma$	$00^04e - 00^00e$	8450.30549(14)	0.39185694(48)	1.6315(27)	R45/P47	68/83	0.64
8747.81028(50)	$\Sigma-\Sigma$	$20^03e - 00^00e$	8747.81028(50)	0.3916801(26)	1.515(28)	R31/P34	50/55	1.6

Note: The lower state constants were fixed at the values of Ref. [6]. The uncertainties are given in parenthesis in the unit of the last quoted digit. In the case of previously analyzed bands, the corresponding spectroscopic parameters are given in italics for comparison: ^aAmiot [5], ^bLyulin [13].

^a Difference between the upper and lower vibrational term values.

^b Normal mode labeling according to the maximum value of the modulo of the expansion coefficients of an eigenfunction. In the cases, when there are two candidates for the same labeling or modulo of two principal expansion coefficients practically coincide, we give in parentheses the second variant of the labeling. Note that as a result of strong mixing among the various vibrational bands, the normal mode labeling of some states differs from that given in the previous analysis.

5750.7230 cm⁻¹ and 5736.8392 cm⁻¹, respectively. The Q-branch of the perpendicular cold band $01^12f - 00^00e$ is shown in Fig. 3.

The plot in Fig. 4 presents our observed bands in this work for the $^{15}\text{N}_2^{16}\text{O}$ isotopologue. The line intensities as provided by the polyad model [10] were adopted for these plots.

3.2. Band-by-band rotational analysis

The standard expression below for the vibration–rotation energy levels was used to determine the spectroscopic parameters:

$$F_v(J) = G_v + B_v J(J+1) - D_v J^2(J+1)^2 + H_v J^3(J+1)^3 \quad (1)$$

In (1), G_v is the vibrational term value, B_v is the rotational constant, D_v and H_v are the centrifugal distortion constants. The spectroscopic parameters for an upper state were fitted directly to the observed line positions of the respective band, and in the case of hot bands involving e and f rotational levels, the $e-e$, $e-f$, $f-e$, and $f-f$ sub-bands were considered independently. The lower state rotational constants were constrained to their literature values [6]. The observed line positions together with the residuals are given in the Supplementary material of this paper. The spectroscopic parameters re-

trieved from the fitting of the line positions are listed in Table 2. For 19 bands, our work looked at transitions of higher J value and gave more accurate spectroscopic constants than Amiot's work [5], which were reviewed and given in Table 2. The RMS values of the deviations of (observed-calculated) are mostly less than 1.0×10^{-3} cm⁻¹, which is consistent with the experimental accuracy of the line positions. Note that the line positions of the R branch of $01^13 - 01^10$ band should be adopted with caution, because the R branch of this band observed in present work was not resolved for the $e-e$ and $f-f$ sub-bands as other isotopologues of nitrous oxide [2,3].

4. Discussion and conclusion

The (observation–prediction) deviations of the line positions of the $^{15}\text{N}_2^{16}\text{O}$ isotopologue assigned in the studied region are illustrated on Fig. 5. The predictive ability of the effective Hamiltonian parameters [10] of the $^{15}\text{N}_2^{16}\text{O}$ isotopologue is good, since the majority of the residuals lies between -0.05 and 0.05 cm⁻¹. However, the accuracy of the modeling of the line positions for this isotopologue is worse than other isotopologues of nitrous oxide such

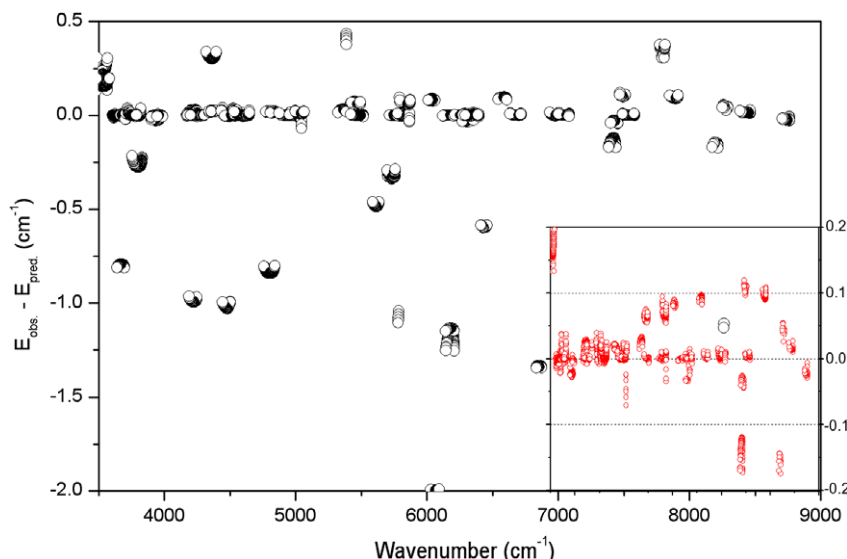


Fig. 5. Difference between the line positions of the $^{15}\text{N}_2^{16}\text{O}$ isotopologue of nitrous oxide between 3500 and 9000 cm⁻¹ and their values predicted by the effective ro-vibrational Hamiltonian [10].

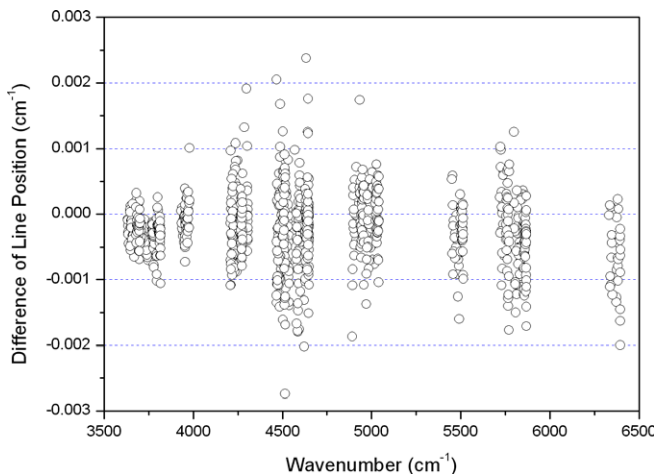


Fig. 6. Difference of the line positions of the $^{15}\text{N}_2^{16}\text{O}$ isotopologue of nitrous oxide in the 3500–9000 cm^{-1} region between this work and Amiot [5].

as $^{14}\text{N}_2^{16}\text{O}$ [11], $^{14}\text{N}^{15}\text{N}^{16}\text{O}$ and $^{14}\text{N}_2^{16}\text{O}$ [4]. Especially, the deviations of the observed line positions from those predicted of the $42^0\text{o}_e - 00^0\text{o}_e$ band centered at $6067.1576 \text{ cm}^{-1}$ exceed 2 cm^{-1} . No doubt that the new observed line positions will be very useful to improve the set of effective Hamiltonian parameters for this isotopic species. Due to no input experimental intensity information, the set of the effective dipole momentum of $^{14}\text{N}_2^{16}\text{O}$ isotopologue [12] was used for $^{15}\text{N}_2^{16}\text{O}$ isotopologue in the calculation. The sensitivity in this work is about $5 \times 10^{-26} \text{ cm}^{-1}/(\text{molecule } \text{cm}^{-2})$, so it is clear from Fig. 4 that the predicted intensities of most bands are underestimated. The subsequent work of experimental line intensity will help to obtain the set of the effective dipole momentum parameters for $^{15}\text{N}_2^{16}\text{O}$ isotopologue.

Fig. 6 gives the difference between the line positions of this isotopologue assigned in this work and Amiot's spectrum between 3500 and 9000 cm^{-1} . The line positions of Amiot [5] have been calibrated by 0.99999983. This figure demonstrates a good agreement between different studies.

Acknowledgments

The authors thank Dr. V.I. Perevalov for providing the predictions on the basis of global effective Hamiltonian models. This

work is jointly supported by NSFC-China (Grant Nos. 20903085, 10574124 and 20873132), by the Fok Ying Tong Education Foundation (101013), and by Chinese Ministry of Science and Technology (2007CB815203).

Appendix A. Supplementary data

Supplementary data for this article are available on ScienceDirect (www.sciencedirect.com) and as part of the Ohio State University Molecular Spectroscopy Archives (http://library.osu.edu/sites/msa/jmsa_hp.htm). Supplementary data associated with this article can be found, in the online version, at doi:[10.1016/j.jms.2009.10.006](https://doi.org/10.1016/j.jms.2009.10.006).

References

- [1] L. Wang, V.I. Perevalov, S.A. Tashkun, B. Gao, L.-Y. Hao, S.-M. Hu, J. Mol. Spectrosc. 237 (2006) 129–136.
- [2] H.-Y. Ni, K.-F. Song, V.I. Perevalov, S.A. Tashkun, A.-W. Liu, L. Wang, S.-M. Hu, J. Mol. Spectrosc. 247 (2008) 64–75.
- [3] K.-F. Song, A.-W. Liu, H.-Y. Ni, S.-M. Hu, J. Mol. Spectrosc. 255 (2009) 24–31.
- [4] C.Y. Wang, A.W. Liu, V.I. Perevalov, S.A. Tashkun, K.F. Song, S.M. Hu, J. Mol. Spectrosc. 257 (2009) 94–104.
- [5] C. Amiot, J. Mol. Spectrosc. 59 (1976) 380–395.
- [6] RA. Toth, Available from: <<http://mark4sun.jpl.nasa.gov/n2o.html>>.
- [7] L.S. Rothman, I.E. Gordon, A. Barbe, D. Chris Benner, P.F. Bernath, M. Birk, V. Boudon, L.R. Brown, A. Campargue, J.-P. Champion, K. Chance, L.H. Couder, V. Dana, V.M. Devi, S. Fally, J.-M. Flaud, R.R. Gamache, A. Goldman, D. Jacquemart, I. Kleiner, N. Lacome, W.J. Lafferty, J.-Y. Mandin, A.V. Nikitin, J. Orphal, V.I. Perevalov, A. Perrin, A. Predoi-Cross, C.P. Rinsland, M. Rotger, M. Šimečková, M.A.H. Smith, K. Sung, S.A. Tashkun, J. Tennyson, R.A. Toth, A.C. Vandaele, J. Vander Auwera, J. Quant. Spectrosc. Radiat. Transfer 110 (2009) 533–572.
- [8] N. Jacquinot-Husson, N.A. Scott, A. Chédin, L. Crépeau, R. Armante, V. Capelle, J. Orphal, A. Coustenis, C. Boone, N. Poulet-Crovisier, A. Barbe, M. Birk, L.R. Brown, C. Camy-Peyret, C. Claveau, K. Chance, N. Christidis, C. Clerbaux, P.F. Coheur, V. Dana, L. Daumont, M.R. De Backer-Barilly, G. Di Lonardo, J.M. Flaud, A. Goldman, A. Hamdouni, M. Hess, M.D. Hurley, D. Jacquemart, I. Kleiner, P. Köpke, J.Y. Mandin, S. Massie, S. Mikhailenko, V. Nemtchinov, A. Nikitin, D. Newnham, A. Perrin, V.I. Perevalov, S. Pinnock, L. Régalia-Jarlot, C.P. Rinsland, A. Rublev, F. Schreier, L. Schult, K.M. Smith, S.A. Tashkun, J.L. Teffo, R.A. Toth, V.I.G. Tyuerev, J. Vander Auwera, P. Varanasi, G. Wagner, J. Quant. Spectrosc. Radiat. Transfer 109 (2008) 1043–1059.
- [9] A.V. Vlasova, B.V. Perevalov, S.A. Tashkun, V.I. Perevalov, Fifteenth Symposium on High Resolution Molecular Spectroscopy, Nizhnii Novgorod, Russia, 18–21 July, Poster D20, 2006, p. 86.
- [10] A.W. Liu, S. Kassi, P. Malara, D. Romanini, V.I. Perevalov, S.A. Tashkun, S.M. Hu, A. Campargue, J. Mol. Spectrosc. 244 (2007) 33–47.
- [11] L. Daumont, J. Vander Auwera, J.-L. Teffo, V.I. Perevalov, S.A. Tashkun, J. Quant. Spectrosc. Radiat. Transfer 104 (2007) 342–356.
- [12] O.M. Lyulin, D. Jacquemart, N. Lacome, S.A. Tashkun, V.I. Perevalov, J. Quant. Spectrosc. Radiat. Transfer, doi:[10.1016/j.jqsrt.2009.10.010](https://doi.org/10.1016/j.jqsrt.2009.10.010).